NANO LETTERS

Letter

pubs.acs.org/NanoLett

Twinning and Twisting of Tri- and Bilayer Graphene

Lola Brown,[†,∥] Robert Hovden,[‡,∥] Pinshane Huang,[‡] Michal Wojcik,[†] David A. Muller,[‡,§] and Jiwoong Park*[,†,§]

[†]Department of Chemistry and Chemical Biology and [‡]School of Applied and Engineering Physics, Cornell University, Ithaca, New York 14853, United States

[§]Kavli Institute at Cornell for Nanoscale Science, Ithaca, New York 14853, United States

Supporting Information

ABSTRACT: The electronic, optical, and mechanical properties of bilayer and trilayer graphene vary with their structure, including the stacking order and relative twist, providing novel ways to realize useful characteristics not available to single layer graphene. However, developing controlled growth of bilayer and trilayer graphene requires efficient large-scale characterization of multilayer graphene structures. Here, we use dark-field transmission electron microscopy for rapid and accurate determination of key structural parameters (twist angle, stacking order, and interlayer spacing) of few-layer CVD graphene. We image the long-range atomic registry for oriented bilayer and trilayer graphene, find that it conforms exclusively to either Bernal or rhombohedral stacking, and determine their relative abundances. In contrast, our data on twisted multilayers suggest the absence of such long-range atomic registry. The atomic registry and its absence are consistent with the two different strain-induced deformations we observe; by tilting the samples to break mirror symmetry, we find a high density of twinned domains in oriented multilayer graphene, where multiple domains of two different stacking configurations coexist, connected by discrete twin boundaries. In contrast, individual layers in twisted regions continuously stretch and shear independently, forming elaborate Moiré patterns. These results, and the twist angle distribution in our CVD graphene, can be understood in terms of an angle-dependent interlayer potential model.

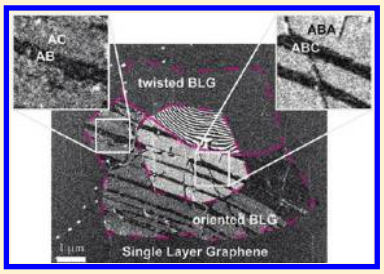

KEYWORDS: *Bilayer graphene, twisted bilayer graphene, dark-field TEM, domain boundary, twin boundary, interlayer interaction*

Bilayer graphene (BLG) and trilayer graphene (TLG) are a prototypical layered material system where interlayer structure and coupling determines key physical properties. Their electronic, optical, and mechanical properties may be varied depending upon their structures, including the stacking order, relative twist, and interlayer spacing,[1−7] providing ways to realize useful characteristics not available to single layer graphene. A well-known example is Bernal-stacked (BS) BLG and rhombohedral TLG, which open tunable band gaps in a transverse electric field;[8−10] making them promising candidates for optoelectronic and nanoelectronic applications. Twisted BLG has also been a subject of many recent studies, both theoretical and experimental, where the interlayer coupling, which is sensitive to the configuration of commensurate unit cell, provides intriguing possibilities for controlling electronic band structure.[11] Furthermore, graphene growth using chemical vapor deposition (CVD) can now produce large areas of single and multilayer graphene,[12−14] which could allow utilization of BLG and TLG in technologically relevant scale. However, the CVD method may grow them in various stacking configurations that are not common in natural graphite, a significant problem because most applications require materials with uniform electrical and optical properties. Controlling stacking and other structural properties in BLG and TLG synthesis thus necessitates efficient large-scale characterization of multilayer graphene structures, which must provide all key structural information. These include the twist angle, stacking configuration, and interlayer spacing as well as local structural deformations.

In this paper, we use dark-field transmission electron microscopy (DF-TEM) and selected area electron diffraction (SAED) techniques for quick, accurate, and high-resolution determination of twist angle, interlayer atomic registry (stacking order), and interlayer spacing of bi- and trilayer CVD graphene. In contrast to Raman mapping[15] and high-resolution TEM,[16] these techniques allow large areas to be mapped and processed in seconds. The accessibility of these techniques, which utilize a common, commercial uncorrected TEM, is particularly appealing. In DF-TEM, real-space images are formed from a selected diffracted beam. These images are sensitive to the alignment between the electron diffraction angle and the crystal orientation and have been used to characterize the grain structure of CVD graphene.[17,18] SAED provides regional structural information and has recently enabled quantification of the intrinsic roughening in exfoliated graphene.[19] We use the SAED peak intensities measured at various diffraction and sample tilt angles which, when combined with DF-TEM imaging, provide a powerful set of

Received: December 25, 2011
Revised: February 7, 2012

dx.doi.org/10.1021/nl204547v | *Nano Lett.* XXXX, XXX, XXX−XXX

information that enables detailed structural characterization in BLG and TLG.

Using this technique, we first find that our CVD growth produces a mixture of BLG and TLG areas both in oriented (non-twisted) and twisted configurations with the oriented ones as the major species. Our data show that the structure of oriented BLG (oBLG) and TLG (oTLG) contain long-range atomic registry and conform exclusively to either Bernal or rhombohedral stacking with the same interlayer spacing as that of natural graphite (3.35 Å). In contrast, we show that twisted BLG (tBLG) lacks long-range atomic registry, and that the twisted layers are free to move laterally with respect to each other, suggesting superlubricity[20] between the top and bottom layers. The atomic registry (and its absence) in oBLG and tBLG is consistent with the two different strain-induced deformations we observed. In oBLG, multiple domains of two different Bernal-stacked configurations (AB vs AC stacking) coexist within individual oBLG pieces connected by discrete twin domain boundaries, while individual layers in tBLG regions continuously stretch and shear independently forming elaborate Moiré patterns. Finally, these results are discussed together with an angle-dependent interlayer potential model, which explains the twist angle distribution in our CVD graphene.

The graphene samples studied in this work was synthesized using the low-pressure CVD method,[12,13] which produces high-quality graphene. Previously, it was shown that this method can be used to grow graphene with a different number of layers and various grain structures by modifying growth parameters, such as reactant gas flow rates and furnace temperature,[21−24] making it an ideal method for producing large scale BLG and TLG samples. Under our growth conditions (see Supporting Information), we observe extended single layer graphene (10−60 μm across) dotted with multilayer regions, whose size ranges between 2 and 7 μm across (see Figure 1d). While SEM images may be used to locate these multilayer regions and to resolve the number of layers in each region (Figure 1a), they provide no other structural information. In order to measure the twist angles in these regions, we transferred the graphene from the Cu growth substrate to a TEM support grid (see Supporting Information for transfer method) and took an SAED image of each region. Multilayer regions are either all in same orientation indicated by the single set of six-fold diffraction peaks (Figure 1b, inset), or arranged in twisted configurations with more than one set of diffraction peaks (Figure 1c, inset), or in a combination of these two options. Once these diffraction spots are identified, DF-TEM images are taken to form spatial images of BLG and TLG regions with an aperture chosen for each electron diffraction spots. The combination of SAED and DF-TEM images thus allow full determination of twist angles in each multilayer graphene area (Figure 1b,c). In Figure 1d, we show the distribution of twist angle and area measured from over a hundred individual bilayer domains in 50 contiguous multilayer sites. We find that in our CVD growth most of the bilayer area is oriented (70%) while only 30% are twisted. An additional histogram is shown in Figure 5.

In both oriented and twisted multilayer graphene, one important question is the presence of interlayer atomic registry (stacking order). If adjacent layers are atomically registered, the $x-y$ position of the two-atom unit cell is specified by a single lateral displacement vector everywhere. For instance, there are several different stacking configurations in oriented multilayer

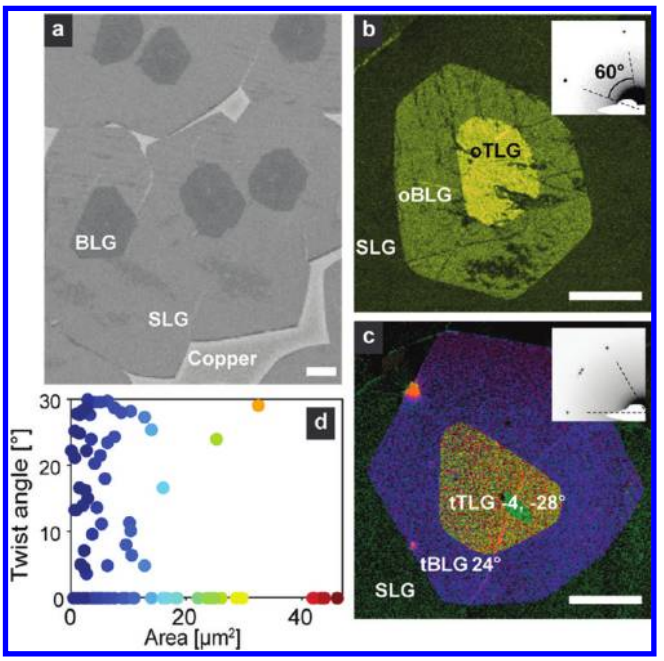

Figure 1. Imaging twist angles in multilayer graphene. (a) SEM image of CVD graphene partially grown on the Cu substrate. (b) DF-TEM image of oriented BLG and TLG. (Inset) Diffraction pattern with one set of peaks within 60°. (c) Three layers that are twisted with respect to each other. (Inset) Diffraction pattern within 60°. Relative twist angles of the second and third layers are labeled in each region. All scale bars are 1 μm. (d) Twist angle−area plot measured for over 100 BLG domains.

graphene. In the typical "graphitic", or "Bernal" stacking commonly found in highly oriented pyrolitic graphite (HOPG),[15] half of the atoms in one layer are positioned exactly on top of half the atoms of the other layer. Two different Bernal stacking arrangements exist for bilayer graphene; for a given basis layer A, the second layer can be either a B or a C layer, each shifted by half a basis vector (arrows, Figure 2a) with respect to each other. Furthermore, for oriented TLG, there are two principle forms, a Bernal (ABA) stacked or rhombohedral (ABC) stacked trilayer. While geometrically similar, these two stacking arrangements can radically change the electronic properties, from tunable bandgaps in Bernal stacked bilayer and rhomboheral trilayer to metallic behaviors in Bernal stacked trilayer.[8,23] Other types of stacking are also possible in oriented multilayer graphene, such as AA stacking.[25] Currently there are no direct studies on the stacking order in CVD multilayer graphene. We use the relative electron diffraction intensity in our DF-TEM images for this purpose. Our results on oriented BLG and TLG are shown in Figures 2 and 3.

In oBLG, the electron diffraction intensities could be larger or smaller than that of a single layer graphene.[19] This is because the electron wave diffracted from one layer interferes with the wave diffracted from the other layer, where the relative phase θ between the two diffracted waves is determined by the lateral shift (Δx) of the lattice lines in the top layer relative to those in the bottom layer. Under the flat Ewald sphere approximation, this leads to fully constructive (or destructive) interference when $\Delta x = 0$ ($\Delta x = 1/2$ lattice period). Using this model, the DF-TEM intensity for the first and second order families of diffraction peaks $Ø_1$ and $Ø_2$ (see Figure 2b) can be estimated for Bernal stacked oBLG. For $Ø_2$ peaks, which corresponds to

dx.doi.org/10.1021/nl204547v | Nano Lett. XXXX, XXX, XXX−XXX

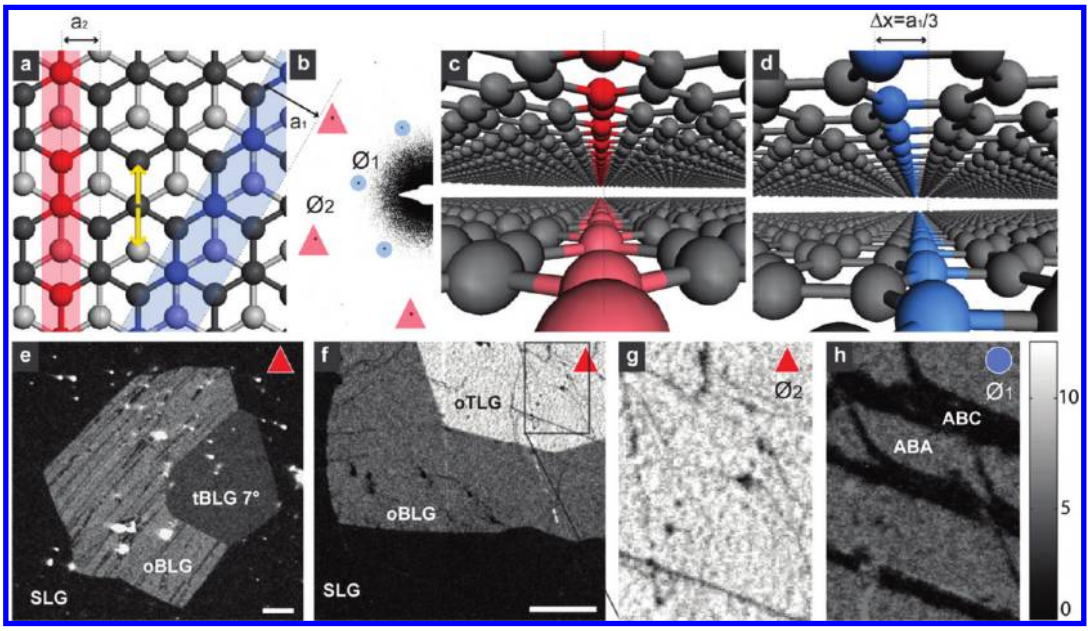

Figure 2. Stacking order in oriented BLG and TLG. (a) Bernal stacked (BS) bilayer. The graphene lattice with period a_2= 1.23 Å (a_1 = 2.13 Å) is highlighted in red (blue). Displacement vectors for AB, or AC configurations are marked in yellow. (b) SAED pattern of BS-BLG. We name the equivalent Bragg reflections $Ø_2$ and $Ø_1$, corresponding to 1.23 and 2.13 Å lattice spacing, respectively. (c) Three-dimensional illustration of BS-BLG 1.23 Å lattice; (d) 3D illustration of BS-BLG 2.13 Å lattice. (e) DF-TEM ($Ø_2$) image of BLG containing two stacking arrangements: a Bernal stacked region and a twisted region (7° rotation). The intensity of the BS region is roughly twice that of the twisted region. (f) DF-TEM ($Ø_2$) of trilayer graphene with graphitic (ABA, ABC, or ACB) stacking; the uniform intensity indicates complete coverage. (g) Close-up of the trilayer area in (f). (h) DF-TEM ($Ø_1$) of the same region shows discrete changes in regional intensity, indicating ABA (bright) and ABC/ACB (dark) stacking. DF-TEM image intensities are normalized to the first layer. All scale bars are 1 μm.

the lattice line periodicity of a_2= 1.23 Å (red lines in Figure 2a,c), fully constructive interference occurs since lattice lines in both top and bottom layers are vertically aligned (Figure 2c). Maximum intensities are expected for all oriented BLG and TLG with graphitic stacking configurations for the same reason, when they are imaged using one of the $Ø_2$ peaks. In contrast, the lattice lines with a longer a_1 = 2.13 Å period (corresponding to $Ø_1$ peaks in Figure 2b) are shifted in the top layer by one-third of the period (Figure 2d), resulting in a phase shift of $\theta = (2\pi)(\Delta x/a_1) = 2\pi/3$. This phase is also highly sensitive to tilts; for the configuration shown in Figure 2d, θ will decrease (increase) with a small clockwise (counter-clockwise) tilt rotation.

We observe these behaviors from the DF-TEM images of our oriented BLG and TLG. In Figure 2e we show a DF-TEM image of an oBLG domain connected to a tBLG (twisted angle = 7°), taken from an $Ø_2$ peak. The oBLG is almost four times as bright as the single layer as a result of fully constructive interference, whereas the rotated bilayer is simply twice as bright. We observe this brighter DF-TEM intensity from any of the six $Ø_2$ peaks for all oBLG areas in our sample, with a uniform intensity. This confirms that CVD grown oBLG has a long-range stacking order and atomic interlayer registry. We also note that this increase in intensity is an efficient way to identify oriented multilayer regions. Furthermore, our measurements show that $Ø_1$ intensities on oBLG (Figure 3) and oTLG (Figure 2h) are consistent with the expected values for graphitic stacking (Bernal or rhombohedral) order, thus excluding the AA stacking. One representative example is shown in Figure 2f–h. They are DF-TEM images of an oriented BLG/TLG region with Figure 2g (taken with a $Ø_2$ peak) and Figure 2h ($Ø_1$) each showing a zoom-in image of the TLG area marked in Figure 2f (also taken with a $Ø_2$ peak). While Figure 2g shows uniformly bright intensity as expected, Figure 2h has sharply defined bright and dark stripes. Because the dark striped regions in Figure 2h maintain the same bright intensity in Figure 2g (roughly 9 times as bright as single layer graphene), they cannot be tears or gaps in the graphene. Instead, the discrete changes in Figure 2h and the uniform intensities in Figure 2g of the oTLG area agree with the expected theoretical intensities for two different graphitic stackings (Figure S3 in Supporting Information), Bernal (ABA; bright stripes in Figure 2h) and rhombohedral (ABC; dark stripes). In particular, the ABC stacked areas show completely destructive interference because the diffracted electron wave from the second and third layer has a relative phase difference of $2\pi/3$ and $4\pi/3$, respectively.

Surprisingly, we observe similar behaviors from Bernal stacked BLG, as shown in Figure 3a,b. The $Ø_2$ image of a Bernal stacked BLG (Figure 3a) shows uniform intensity, incorrectly suggesting a continuously stacked second layer, whereas the $Ø_1$ image of the same area (Figure 3b) display sharply contrasted bright and dark stripes. These structures with discrete changes in the $Ø_1$ intensity are abundant across all of our oBLG samples; they are often observed along parallel lines (Figure 3b,c), or in complex orientations (Figure 3d), while few BS regions do not display them at all (Figure 3e). We ascribe these behaviors to the presence of two distinct Bernal stacked configurations (AB and AC) coexisting within single oBLG domains. As explained earlier, they are associated with two different displacement vectors (Figure 2a) and are mirrored configurations. When the BLG sample is perpendicular to the incoming electron beam, the two configurations are identical and cannot be distinguished. However, a slight tilting of the sample may break the mirror symmetry resulting in different $Ø_1$ peak intensities. To resolve the difference between

dx.doi.org/10.1021/nl204547v | Nano Lett. XXXX, XXX, XXX–XXX

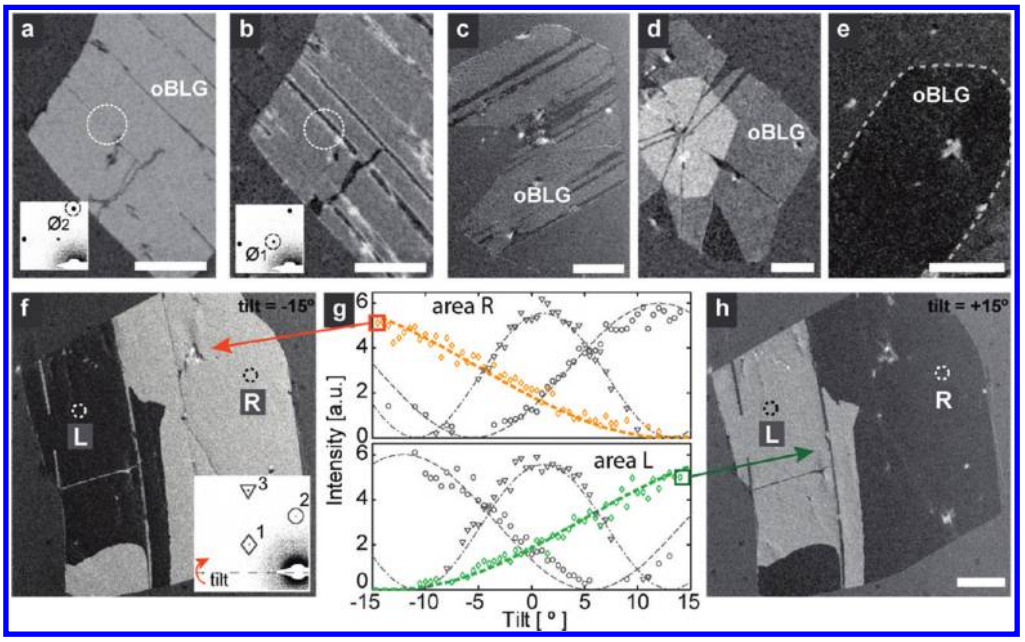

Figure 3. Twinning in oriented BLG. (a) DF-TEM ($Ø_2$) image of BS-BLG, with uniform intensity. (Inset) Diffraction pattern. (b) DF-TEM ($Ø_1$) image of the same area in (a) shows sharp contrast from AB/AC twinning across the bilayer region. (Inset) Diffraction pattern. (c–e) Other examples ($Ø_1$) of twinning in BS bilayer graphene. oBLG border is marked in a dotted line in (e) for clarity. (f) DF-TEM image showing AB/AC twinning of a BS-BLG tilted −15° relative to the incident beam. Image was taken with diffraction peak #1, indicated in the inset. (Inset) Diffraction pattern taken at 0° tilt, showing the $Ø_1$ peaks 1 (diamond) and 2 (circle) and $Ø_2$ peak 3 (triangle). (g) Integrated intensity of diffraction spots 1–3 as a function of tilt angle taken from regions R and L as marked in (f,h). Integrated intensity was determined from a 6-parameter 2D Gaussian fit. The dashed lines are theoretical intensities calculated for BS-BLG and an 80 keV electron beam. The curves corresponding to spot no. 1 location are marked in orange (area R) and green (area L) to highlight the mirrored symmetry in the twinned regions. (h) DF-TEM image of the same area as (f) taken with diffraction spot no. 1 at +15° tilt. All scale bars are 1 μm.

the AB and AC mirrored configurations in BLG, one may thus exploit the sensitivity of the $Ø_1$ peak to sample tilt angle relative to the electron beam. Most of our oBLG samples are indeed not perfectly perpendicular to the electron beam axis, which explains the significant contrast observed in Figure 3b–e.

We confirm that these are Bernal stacked AB/AC crystalline twins by performing a tilt-dependent SAED analysis on two of these areas, as shown in Figure 3g. It plots the total intensity of diffraction spots 1, 2, and 3 (Figure 3f, inset), as a function of tilt angle for the twinned locations L and R shown in Figure 3f,h. One can see that the two $Ø_1$ peaks (1-diamond and 2-circle) express the mirrored behavior of the twinned regions, while the $Ø_2$ peak (3-triangle) remains similar in both AB and AC stacking. This result is in agreement with previous discussion and our full theoretical calculation of the diffraction spot tilt pattern, determined from the scattered wave function of Bernal stacked graphene (see Figure S3 and methods, Supporting Information). The corresponding DF image intensity for each twinning regions of the BLG indeed varies with tilt angles − as demonstrated in Figure 3f,h − measured with tilt angles ±15°. These images clearly show twinning of oBLG. Furthermore, we can estimate the interlayer spacing in the Bernal stacked BLG by comparing our experimental SAED tilt data in Figure 3g and theoretical plots. Our analysis based on the plot using diffraction spot 2 in Figure 3g results in 3.27 ± 0.18 Å, close to the 3.35 Å interlayer spacing for HOPG.[26]

Our data shown in Figures 2 and 3 clearly demonstrate for the first time in CVD graphene that non-twisted TLG and BLG areas may contain crystalline twin boundaries. Since these twinning sites are not apparent from SAED without sample tilt, they may be easily mistaken for a single Bernal-stacked domain. In oTLG, we show that a single continuous trilayer region can be composed of both Bernal stacked (ABA) and rhombohedral (ABC) stacked regions, or their permutations, connected by a twin boundary. Similarly, in oBLG, mirrored twins of AB and AC stacked regions are also joined by twin boundaries. We note that this technique provides relative stacking information and does not determine in which layer the twinning occurs. However, it may be possible to infer twinned layers in multilayer systems through continuity with neighboring regions.

Tilted DF-TEM imaging of many samples revealed widely prevalent twinning in our CVD graphene. We propose that the twins observed here are gliding twins, where non-twinned graphene layers slide into a twin position under structural strain present during growth and subsequent cooling.[27] Such strain could be induced by the graphene interaction with features in the Cu substrate, such as steps,[28] or twin boundaries in Cu.[29] Our AFM measurements show that the twin boundaries correspond to a heightened surface line (Figure S2 in Supporting Information). This height deformation may also account for their appearance as dark lines in an $Ø_2$ DF-TEM image (see Figure 3a). Since previous work has demonstrated that twin boundaries on single-layer graphene exhibit structural corrugation and local changes in the densities of states,[29] we expect presence of twins in bilayer graphene will also influence electrical and mechanical properties of Bernal stacked graphene. Controlling these twinning sites will be crucial for device applications.

Now we discuss the structure of twisted multilayer graphene grown using the CVD method. As discussed earlier, the electronic and mechanical properties of tBLG are expected to depend on the interlayer coupling, which in turn is predicted to depend strongly on the commensurability of each twist angle.[4]

dx.doi.org/10.1021/nl204547v | Nano Lett. XXXX, XXX, XXX–XXX

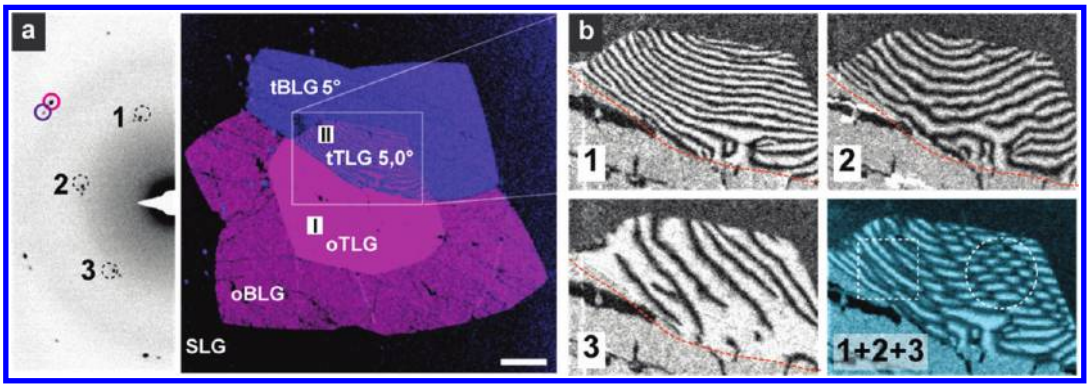

Figure 4. Superlubricity in twisted BLG. (a) DF-TEM color-overlay image of a three layer system taken from two $Ø_2$ diffraction peaks (pink, blue) shown left. Region I shows a three layer graphitic stacking, and region II shows two oriented layers (top and bottom), separated by a twisted middle layer (blue, twist angle is 5°).The Moiré pattern in region II indicates continuous lateral displacement between the top and bottom layers. Scale bar is 1 μm. (b) DF-TEM of the area marked in (a), taken from diffraction peaks 1, 2, and 3, excluding the peak diffracted by the rotated middle layer. The Moiré pattern is indicative of strain. The dashed line in images 1, 2, and 3 shows the boundary between region II and the graphitic region I. The bottom right image is a superposition of the other three images, where an area with isotropic (anisotropic) strain is marked by a circle (square).

Since the size of the commensurate unit cell, an important parameter determining the interlayer coupling, fluctuates wildly for a small angle change, the band structure of tBLG for a given angle remains difficult to predict. One important assumption for most existing theories for high-angle tBLG is that the configuration may be described by a set of discrete parameters (such as p, q indices used by Mele[4]), while treating the lattice constant of both layers as a fixed value. The TEM data shown in Figure 4, however, suggest that such assumption might not be valid in CVD graphene. Instead, our measurements provide strong evidence for superlubricity in twisted multilayer graphene systems.

In Figure 4, we show DF-TEM images of commonly found trilayers AtA stacking system, where "t" denotes a twisted layer. In Figure 4a (left), we show SAED pattern taken from trilayer regions I and II (DF-TEM image, right) together; the SAED pattern shows the major diffraction peaks (including three peaks marked 1, 2, and 3) for the oriented graphene layers (colored pink in the DF-TEM image) and a set of weak spots corresponding to the rotated second layer (blue). When imaged using a major diffraction peak, the DF-TEM images of region I show the behaviors discussed previously, consistent with the atomic registry and uniform intensity within each domain. However, under the same imaging conditions, the intensity in region II presents a complex and continuously varying sinusoidal pattern, as shown in Figure 4b. We conclude that this is a trilayer system with an AtA trilayer (region II) where the middle layer is rotated by 5°, adjoining an oriented TLG (region I). The relative sizes of the three layers are indicative of the slower rates growth rates for the second and the third layer and support the proposed AtA structure for region II.

In general, two twisted layers are predicted to present a Moiré pattern,[30−32] an interference pattern between two mismatched grids. However, twist bilayers with a few degrees of rotation angle show a Moiré periodicity of a few nanometers, too small to easily resolve in DF-TEM imaging. As a result, the tBLG in Figure 2e appears uniform in the DF image despite its relatively small twist angle. When two layers have very similar orientations, such as the outer two layers in region II in Figure 4a, the Moiré periodicity becomes large and will eventually diverge for oriented bilayers if they have long-range atomic registry. Instead, the AtA region in Figure 4a shows the complex Moiré pattern even though the outer two layers have the same orientation. This suggests that there are small lattice mismatches between the top and bottom layers, whose mismatch parameters are continuously varying (as opposed to discrete changes in Figures 3 and 4). This strongly suggests that these aligned "A" layers lack atomic registry or definite stacking order. We propose that this is a result of the lack of atomic registry between the twisted A−t bilayers, due to these constituting layers (both A−t and t−A) being free to move laterally relative to each other, as a result of very low friction, or superlubrication. The Moiré periodicities we observe in Figure 4b are of the order of a few hundred nanometers, indicating strain between A−A layers is on the order of 0.1%. This indication of a spatially varying lattice mismatch in one of the "A" layers results in incommensurate structures for the A−t twisted bilayers. This observation could help explain some of the discrepancies between modeling and experiments in tBLG.

Under this model, the Moiré fringes in Figure 4a may also provide information on local strains which differ between the two separated A−A layers. We further analyze the strain by imaging region II with different $Ø_1$ peaks, as shown in Figure 4b. In each image we see different Moiré patterns, which indicate strain along the direction of the diffraction peak, as well as shear. The strain is highest perpendicular to the boundary between region I and region II (~0.2%) and much lower parallel to it (~0.01%), as seen in Figure 4b-1. Because pure strain would result in Moiré fringes only along the direction of each diffraction peak, the curvature of the lines in Figure 4b-2 indicates that both pure-strain and shear-strain elements are present. Furthermore, by superimposing all three interference images together (Figure 4b, bottom right), we can map out the degree of anisotropy in the strain field. As expected, it is highly anisotropic near the boundary between regions I and II, and become more isotropic away from it. The capability of imaging strain distribution in multilayer graphene, as demonstrated here will be an important characterization method for understanding the mechanical and electrical properties of CVD multilayer graphene devices.

The presence of atomic registry in oBLG and superlubricity in tBLG provides an important clue for explaining the observed twist angle distribution in our CVD multilayers. In Figure 5, we plot area probability histogram compiled based on all our TEM measurements acquired using multiple CVD graphene samples. As discussed earlier, more than 70% of the BLG areas are oBLG

dx.doi.org/10.1021/nl204547v | Nano Lett. XXXX, XXX, XXX−XXX

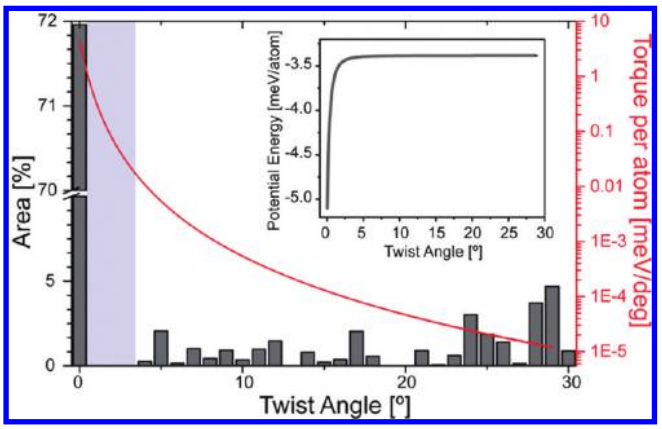

Figure 5. Statistical analysis of twist angle distribution in bilayer graphene. Area probability histogram of bilayer twist angles taken from 50 continuous bilayer regions with >100 individual bilayers. Overlaid in red is the torque calculated based on the theoretical plot of the interlayer potential as a function of the twist angle (inset, as adapted from Morell et al.[6]).

with the rest being tBLG. Two additional trends are seen. We observe no tBLG areas with a twist angle smaller than 4° (shaded area in Figure 5) and find that the majority (81% of tBLG) of tBLG areas are directly connected to at least one oBLG region (examples in Figure S5, Supporting Information). It is well-known that the Bernal stacked oBLG is the most energetically preferred BLG structure.[6] A theoretical plot of calculated interlayer potential as a function of the twist angle is shown in the inset of Figure 5 (adapted from Morell et al.[6]). It suggests that during growth, tBLG will be subjected to torque, which would drive it toward smaller twist angles. The magnitude of the torque is proportional to the derivative of the interlayer potential and thus increases rapidly near the zero-angle. The depletion of tBLG for small twist angles is consistent with this picture. In addition, the lack of atomic registry in tBLG suggests a lower potential barrier, if any, against rotations driven by this torque, making tBLG unstable when it is not connected to oBLG regions.

In conclusion, we have used SAED and DF-TEM to resolve key structural parameters, including twist angle, stacking configurations, and interlayer spacing in oriented and twisted BLG and TLG grown by CVD method. We find that different stacking configurations with long-range atomic registry coexist in oriented BLG and TLG forming twin boundaries. Similar twinning boundaries are abundant in other macroscopic and nanoscale materials, and their properties and topological structures will be exciting to study in the future. In contrast, the lack of atomic registry in twisted graphene as discussed here suggest new theoretical approaches would be desirable in the description of tBLG. Furthermore, our model based on the interlayer potential and superlubricity in tBLG will be helpful in providing guidelines for controlling the coverage distribution of BLG and TLG with known twist angle by modifying the thermodynamic driving force and kinetics during the growth.

■ ASSOCIATED CONTENT

Ⓢ Supporting Information

Experimental details, diffraction spot analysis, SEM images of Cu steps under graphene, corresponding TEM and AFM images of trilayer graphene, TEM images of other trilayer graphene systems described but not displayed in the main text. This material is available free of charge via the Internet at http://pubs.acs.org.

■ AUTHOR INFORMATION

Corresponding Author

*E-mail: jpark@cornell.edu.

Author Contributions

‖These authors contribute equally to the work.

Notes

The authors declare no competing financial interest.

■ ACKNOWLEDGMENTS

The authors thank J. Kevek for help with sample fabrication and C. S. Ruiz-Vargas for help with AFM imaging. Authors also acknowledge Paul Cueva and Ye Zhu for helpful discussions. This work was mainly supported by AFOSR Grants (FA9550-09-1-0691, FA9550-10-1-0410). L.B. was partially supported by a Fulbright scholarship, R.H. was supported by the Center for Nanoscale Systems, an NSF NSEC (NSF No. EEC-0117770, 0646547), and P.Y.H. was supported by the NSF through the CCMR (NSF DMR-1120296) and an NSF Graduate Research Fellowship (DGE-0707428). This work made use of the TEM facility of the Cornell Center for Materials Research (CCMR) with support from the National Science Foundation Materials Research Science and Engineering Centers (MRSEC) program (DMR 1120296). Sample fabrication was performed at the Cornell Nano-Scale Science and Technology Facility. This research is also partially funded by the Sloan Research Fellowship (J.P.).

■ REFERENCES

(1) Luican, A.; Li, G.; Reina, A.; Kong, J.; Nair, R.; Novoselov, K.; Geim, A.; Andrei, E. Single-Layer Behavior and Its Breakdown in Twisted Graphene Layers. *Phys. Rev. Lett.* **2011**, *106*, 126802.

(2) Lopes dos Santos, J. M. B.; Peres, N. M. R.; Castro Neto, A. H. Graphene Bilayer with a Twist: Electronic Structure. *Phys. Rev. Lett.* **2007**, *99*, 216802.

(3) Shallcross, S.; Sharma, S.; Landgraf, W.; Pankratov, O. Electronic structure of graphene twist stacks. *Phys. Rev. B* **2011**, *83*, 054502.

(4) Mele, E. J. Commensuration and interlayer coherence in twisted bilayer graphene. *Phys. Rev. B* **2010**, *81*, 161405R.

(5) Ohta, T.; Bostwick, A.; Seyller, T.; Horn, K.; Rotenberg, E. Controlling the electronic structure of bilayer graphene. *Science (New York, N.Y.)* **2006**, *313*, 951−4.

(6) Suárez Morell, E.; Vargas, P.; Chico, L.; Brey, L. Charge redistribution and interlayer coupling in twisted bilayer graphene under electric fields. *Phys. Rev. B* **2011**, *84*, 195421.

(7) Hicks, J.; Sprinkle, M.; Shepperd, K.; Wang, F.; Tejeda, A.; Taleb-Ibrahimi, A.; Bertran, F.; Le Fèvre, P.; de Heer, W.; Berger, C.; Conrad, E. Symmetry breaking in commensurate graphene rotational stacking: Comparison of theory and experiment. *Phys. Rev. B* **2011**, *83*, 205403.

(8) Lui, C. H.; Li, Z.; Mak, K. F.; Cappelluti, E.; Heinz, T. F. Observation of an electrically tunable band gap in trilayer graphene. *Nat. Phys.* **2011**, *7*, 944−947.

(9) Castro, E.; Novoselov, K.; Morozov, S.; Peres, N.; dos Santos, J.; Nilsson, J.; Guinea, F.; Geim, A.; Neto, A. Biased Bilayer Graphene: Semiconductor with a Gap Tunable by the Electric Field Effect. *Phys. Rev. Lett.* **2007**, *99*, 216802.

(10) Zhang, Y.; Tang, T.-T.; Girit, C.; Hao, Z.; Martin, M. C.; Zettl, A.; Crommie, M. F.; Shen, Y. R.; Wang, F. Direct observation of a widely tunable bandgap in bilayer graphene. *Nature* **2009**, *459*, 820−3.

(11) MacDonald, A. H.; Bistritzer, R. Materials science: Graphene moiré mystery solved? *Nature* **2011**, *474*, 453−4.

(12) Li, X.; Magnuson, C. W.; Venugopal, A.; Tromp, R. M.; Hannon, J. B.; Vogel, E. M.; Colombo, L.; Ruoff, R. S. Large-area graphene single crystals grown by low-pressure chemical vapor deposition of methane on copper. *J. Am. Chem. Soc.* **2011**, *133*, 2816−9.
(13) Bae, S.; Kim, H.; Lee, Y.; Xu, X.; Park, J.-S.; Zheng, Y.; Balakrishnan, J.; Lei, T.; Kim, H. R.; Song, Y. I.; Kim, Y.-J.; Kim, K. S.; Ozyilmaz, B.; Ahn, J.-H.; Hong, B. H.; Iijima, S. Roll-to-roll production of 30-in. graphene films for transparent electrodes. *Nat. Nanotechnol.* **2010**, *5*, 574−8.
(14) Reina, A.; Jia, X.; Ho, J.; Nezich, D.; Son, H.; Bulovic, V.; Dresselhaus, M. S.; Kong, J. Large area, few-layer graphene films on arbitrary substrates by chemical vapor deposition. *Nano Lett.* **2009**, *9*, 30−5.
(15) Lui, C. H.; Li, Z.; Chen, Z.; Klimov, P. V.; Brus, L. E.; Heinz, T. F. Imaging stacking order in few-layer graphene. *Nano Lett.* **2011**, *11*, 164−9.
(16) Nelson, F.; Diebold, A. C.; Hull, R. Simulation Study of Aberration-Corrected High-Resolution Transmission Electron Microscopy Imaging of Few-Layer-Graphene Stacking. *Microsc. Microanal.* **2010**, *16*, 194−199.
(17) Huang, P. Y.; Ruiz-Vargas, C. S.; van der Zande, A. M.; Whitney, W. S.; Levendorf, M. P.; Kevek, J. W.; Garg, S.; Alden, J. S.; Hustedt, C. J.; Zhu, Y.; Park, J.; McEuen, P. L.; Muller, D. A. Grains and grain boundaries in single-layer graphene atomic patchwork quilts. *Nature* **2011**, *469*, 389−92.
(18) Kim, K.; Lee, Z.; Regan, W.; Kisielowski, C.; Crommie, M. F.; Zettl, A. Grain boundary mapping in polycrystalline graphene. *ACS Nano* **2011**, *5*, 2142−6.
(19) Meyer, J. C.; Geim, A. K.; Katsnelson, M. I.; Novoselov, K. S.; Booth, T. J.; Roth, S. The structure of suspended graphene sheets. *Nature* **2007**, *446*, 60−3.
(20) Dienwiebel, M.; Verhoeven, G.; Pradeep, N.; Frenken, J.; Heimberg, J.; Zandbergen, H. Superlubricity of Graphite. *Phys. Rev. Lett.* **2004**, *92*.
(21) Yan, K.; Peng, H.; Zhou, Y.; Li, H.; Liu, Z. Formation of bilayer bernal graphene: layer-by-layer epitaxy via chemical vapor deposition. *Nano Lett.* **2011**, *11*, 1106−10.
(22) Yu, Q.; Jauregui, L. A.; Wu, W.; Colby, R.; Tian, J.; Su, Z.; Cao, H.; Liu, Z.; Pandey, D.; Wei, D.; Chung, T. F.; Peng, P.; Guisinger, N. P.; Stach, E. A.; Bao, J.; Pei, S.-S.; Chen, Y. P. Control and characterization of individual grains and grain boundaries in graphene grown by chemical vapour deposition. *Nat. Mater.* **2011**, *10*, 443−9.
(23) Jhang, S.; Craciun, M.; Schmidmeier, S.; Tokumitsu, S.; Russo, S.; Yamamoto, M.; Skourski, Y.; Wosnitza, J.; Tarucha, S.; Eroms, J.; Strunk, C. Stacking-order dependent transport properties of trilayer graphene. *Phys. Rev. B* **2011**, *84*, 116408.
(24) Lee, S.; Lee, K.; Zhong, Z. Wafer scale homogeneous bilayer graphene films by chemical vapor deposition. *Nano Lett.* **2010**, *10*, 4702−7.
(25) Liu, Z.; Suenaga, K.; Harris, P.; Iijima, S. Open and Closed Edges of Graphene Layers. *Phys. Rev. Lett.* **2009**, *102*, 015501.
(26) Bacon, G. E. The interlayer spacing of graphite. *Acta Crystallogr.* **1951**, *4*, 558−561.
(27) Lalena, J. N.; Cleary, D. A.; Weiser, M. W. *Principles of Inorganic Materials Design*, 2nd ed.; John Wiley and Sons; New York, 2010; p 585.
(28) Ruiz-Vargas, C. S.; Zhuang, H. L.; Huang, P. Y.; van der Zande, A. M.; Garg, S.; McEuen, P. L.; Muller, D. A.; Hennig, R. G.; Park, J. Softened elastic response and unzipping in chemical vapor deposition graphene membranes. *Nano Lett.* **2011**, *11*, 2259−63.
(29) Lahiri, J.; Lin, Y.; Bozkurt, P.; Oleynik, I. I.; Batzill, M. An extended defect in graphene as a metallic wire. *Nat. Nanotechnol.* **2010**, *5*, 326−9.
(30) Mele, E. J. Interlayer coupling in rotationally faulted multilayer graphenes. *arxiv.org* 2011, 23.
(31) Kaczér, J.; Kroupa, F. The determination of strain by mechanical interference. *Czech. J. Phys.* **1952**, *1*, 80−85.
(32) Hashimoto, H.; Uyeda, R. Detection of dislocation by the Moiré pattern in electron micrographs. *Acta Crystallogr.* **1957**, *10*, 143−143.